A consistency analysis of phase-locked-loop testing and control-based continuation for a geometrically nonlinear frictional system

A Consistency Analysis of Phase-Locked-Loop Testing and Control-Based Continuation for a Geometrically Nonlinear Frictional System

G. Abeloos*[a], F. Müller[b], E. Ferhatoglu[c], M. Scheel[b], C. Collette[a], G. Kerschen[a], M.R.W. Brake[d], P. Tiso[e], L. Renson[f], and M. Krack[b]

[a] *Department of Aerospace and Mechanical Engineering, University of Liège, Belgium*
[b] *Institute for Aircraft Propulsion Systems, University of Stuttgart, Germany*
[c] *Department of Mechanical and Aerospace Engineering, Politecnico di Torino, Italy*
[d] *Department of Mechanical Engineering, Rice University, USA*
[e] *Department of Mechanical and Process Engineering, ETH Zurich, Switzerland*
[f] *Department of Mechanical Engineering, Imperial College London, UK*

Abstract

Two of the most popular vibration testing methods for nonlinear structures are control-based continuation and phase-locked-loop testing. In this paper, they are directly compared on the same benchmark system, for the first time, to demonstrate their general capabilities and to discuss practical implementation aspects. The considered system, which is specifically designed for this study, is a slightly arched beam clamped at both ends via bolted joints. It exhibits a pronounced softening-hardening behavior as well as an increasing damping characteristic due to the frictional clamping. Both methods are implemented to identify periodic responses at steady-state constituting the phase-resonant backbone curve and nonlinear frequency response curves. To ensure coherent results, the repetition variability is thoroughly assessed via an uncertainty analysis. It is concluded that the methods are in excellent agreement, taking into account the inherent repetition variability of the system.

Keywords: Experimental characterization, Nonlinear frequency response, Nonlinear mode backbone, Phase-locked loop testing, Control-based continuation

*Corresponding author.
E-mail addresses: gaetan.abeloos@uliege.be (G. Abeloos), florian.mueller@ila.uni-stuttgart.de (F. Müller), erhan.ferhatoglu@polito.it (E. Ferhatoglu), maren.scheel@ila.uni-stuttgart.de (M. Scheel), christophe.collette@uliege.be (C. Collette), g.kerschen@uliege.be (G. Kerschen), brake@rice.edu (M.R.W. Brake), ptiso@ethz.ch (P. Tiso), l.renson@imperial.ac.uk (L. Renson), malte.krack@ila.uni-stuttgart.de (M. Krack)

Abbreviations

CBC	Control-Based Continuation
FRC	Frequency Response Curve
LP filter	Low-pass filter
NNM	Nonlinear Normal Mode
P	Proportional
PD	Proportional and Differential
PID	Proportional, Integral and Differential
PLL	Phase-Locked Loop
RCT	Response-controlled stepped-sine testing
SSI	Shaker-Structure Interaction

Mathematical symbols

v	Velocity at the measurement point
f	Force applied on the structure, also called excitation
u	Voltage sent to the shaker's amplifier
N	Number of harmonics considered
$\hat{\alpha}_{x,n}$	n^{th} sine Fourier coefficient of the signal x
$\hat{\beta}_{x,n}$	n^{th} cosine Fourier coefficient of the signal x
θ	Instantaneous phase of the voltage
Ω	Excitation frequency
ω	Nonlinear natural frequency
ω_0	Linear natural frequency
ϕ_v	Phase lag between the excitation and the first harmonic of v
X_n	Amplitude of the nth harmonic of a multiharmonic signal x
h	Thickness of the beam

1 Introduction

Experimental characterization of structures is essential to calibrate and validate theoretical models [1] even though laboratory conditions rarely capture operational conditions. Dynamic testing techniques for linear systems can now be considered mature and straightforward, as they have been widely studied in the structural dynamics community over the last decades [2, 3, 4] and are now routinely used in the industry [5]. Experimental techniques are set to play a key role in the development and validation of nonlinear models because of the immense variety in the sources of nonlinear behavior (joints, material, geometry, etc.) and in the nonlinear behaviors themselves. In some circumstances, conventional testing methods can be adequate to test nonlinear structures and

extract some of their dynamic features. For instance, nonlinear frequency responses can be accurately obtained by exploiting successive frequency sweeps performed with an increasing and a decreasing order [6, 7]. The time-domain Hilbert transform [8] applied to structures in free decay is another example. Methods relying on free decay necessitates finding and temporarily maintaining the structure at resonance, which can be difficult to do. The free decay can then follow a non-trivial path through different resonant branches separated by transient jumps [9]. For more complex nonlinear behavior, model-based methods are powerful but strongly depend on the modelling assumptions. For instance, a frequency-domain nonlinear subspace identification can be exploited to identify the parameters of a nonlinear model after exciting the system with random excitation at different constant RMS force levels [10]. The frequency response is subsequently computed from the model using for instance the harmonic balance method [11]. The wide range of nonlinear sources and the potentially high number of parameters render model-based methods difficult to scale to more complex systems, and random excitation might not trigger high-amplitude nonlinear effects.

Consequently, there is a strong need to develop methods to generally and reliably characterize structures with a wide range of complex nonlinear behavior without the need for a model. Some of these behaviors are presented using a single-degree-of-freedom oscillator describing a mode of the physical experiment described in Section 2 with higher damping for readability. The equation of this oscillator is

$$\ddot{x}(t) + 2\xi\omega_0\dot{x}(t) + \omega_0^2 x(t) + k_2 x^2(t) + k_3 x^3(t) = p\sin(\Omega t), \tag{1}$$

where $\xi = 0.8\%$, $\omega_0 = 2178$, $k_2 = 1.9 \times 10^{10}$, $k_3 = 4.1 \times 10^{13}$, and where the right-hand side term represents a harmonic excitation with amplitude p and frequency Ω. The purpose of this model is not to predict experimental results quantitatively but merely to illustrate the concepts presented in this article. Fig. 1 shows the periodic responses of the oscillator for a range of excitation frequencies and amplitudes computed using the harmonic balance method [11] with one harmonic. The response is represented by the amplitude X_1 and phase ϕ_x of its fundamental harmonic component. Responses other than periodic are outside the scope of the present study.

The collection of periodic responses obtained at a constant excitation amplitude defines one of the frequency response curves (FRC) of the system (blue in Fig. 1). Although FRCs usually depict the total response amplitude, this article studies systems that respond primarily through the first harmonic, i.e. that are excited close to a primary resonance without modal interaction. The FRCs in this article therefore depict the relation between the excitation frequency and the first harmonic amplitude. The periodic response with maximum amplitude along a FRC is called the amplitude resonance. In general, it must be distinguished from the phase resonance where the response and excitation satisfy a phase quadrature condition. However, both types of resonances coincide well

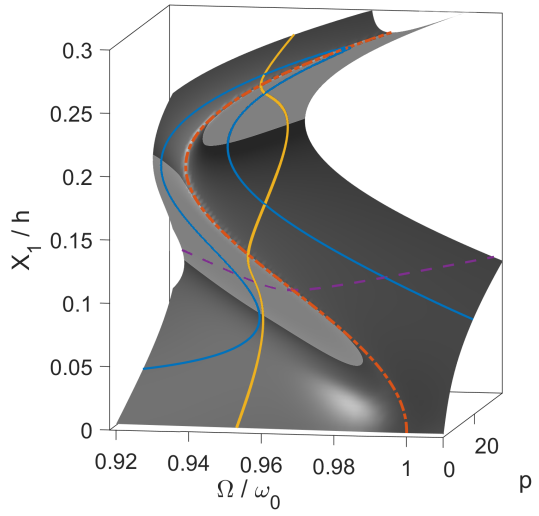

(a)

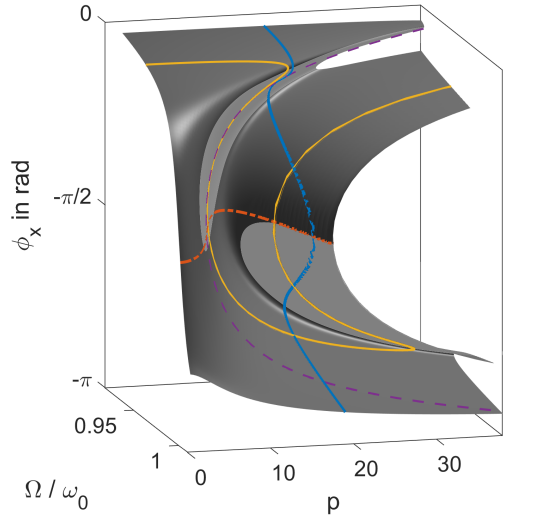

(b)

Figure 1: Response surface representing the periodic responses of the example model (1) by (a) amplitude or (b) phase lag of the fundamental harmonic for varying excitation frequencies and amplitudes, with highlighted FRC (blue curve), S-curve (yellow curve), backbone curve (dash-dot orange curve), and constant-response FRF (dashed purple curve) and unstable responses in lighter grey

for systems with well-separated natural frequencies and light damping, as it is the case in this study. In Fig. 1b, phase-resonant responses are represented by a dash-dot orange curve and have a phase ϕ_x equal to $-\pi/2$. In Fig. 1a, phase-resonant responses form the so-called backbone curve of the system. The backbone curve is the frequency-amplitude relation of a nonlinear normal mode (NNM) [12], and has been used for nonlinear model updating and parameter estimation [13, 14].

The FRC and the backbone curve shown in Fig. 1a highlight some of the key challenges in the experimental characterization of nonlinear structures using testing methods for linear systems.

1. The resonance frequency of nonlinear systems is amplitude-dependent. Here, the example model (1) has a softening-hardening nonlinearity which results in a backbone curve that first decreases in frequency with the response amplitude and then increases after a turning point, as shown in Fig. 1a. As the amplitude-dependent resonance frequency cannot be predicted using linear modal analysis, reaching the resonance of this system using linear techniques would typically require to tune manually the excitation frequency at every excitation amplitude.

2. For a single choice of excitation parameters p and Ω, Fig. 1 shows that the system can exhibit different responses. As a consequence, a slight perturbation on the system can trigger the so-called jump phenomenon during which the response suddenly changes from one steady state response to another. Jumps in an experiment can result in an incomplete characterization of the dynamics, repeatability issues, and even damages to the testing equipment.

3. Some periodic responses are unstable and cannot be identified experimentally without control. The regions where unstable responses exist are enclosed by curves of saddle-node bifurcations and highlighted in light grey in Fig. 1. Fig. 1 also shows that the backbone curve is usually very close to the instability boundary, rendering its identification potentially difficult with traditional methods.

4. When unstable responses cannot be measured, curves of stable responses are disconnected from each other. As such, it might be unclear how they are meant to connect with each other and if any additional feature is present between the curves. For instance, the example model (1) exhibit FRCs whose maximum amplitude may be reached neither by forward nor backward frequency stepping or sweeping. Indeed, both directions encounter a bifurcation point leading to a jump towards a lower amplitude branch, as illustrated in Fig. 2.

An emerging practice to address the challenges introduced by nonlinearity without requiring building a model is to implement feedback control in the ex-

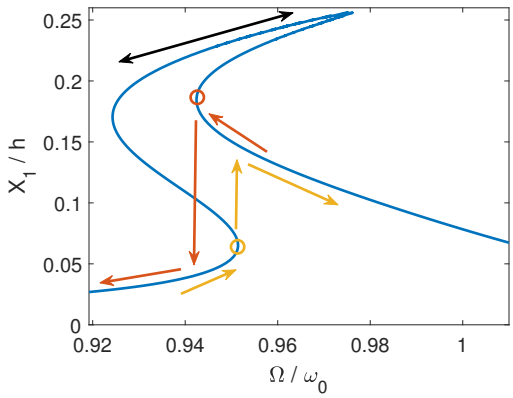

Figure 2: One FRC of the example model (1) exhibiting a stable branch (black arrow) that could be left unidentified when performing a frequency sweep up (yellow arrows) or down (orange arrows) due to meeting bifurcation points (circles)

periment. This ensures more systematic and robust tests [15, 16] because transitions between different regimes of motion can be controlled by the experimenter. The use of feedback control enables the identification of responses around fold bifurcations [17] and responses difficult to reach with classical methods [18], to observe unstable responses [19] and to characterise bifurcations experimentally [20]. Unstable responses and bifurcations are important features of the dynamics. For instance, unstable responses separate the phase space, i.e. they are the boundaries between different types of behavior, and can be used to determine the perturbation size leading to jump between solutions. With control, the complete nonlinear response of the system can be captured directly and without requiring models during the experiments. When using classical experimental techniques, this is only possible through post-processing [8]. Three methods for feedback-controlled testing of nonlinear structures are control-based continuation, phase-locked loop testing, and response-controlled stepped-sine testing.

Control-based continuation (CBC) is a means to apply the principles of numerical continuation directly to a physical system [16]. CBC is a general technique that has been used in many experiments to steer and maintain the dynamics of a physical system around a periodic but otherwise arbitrary prescribed target response using feedback control [21, 22, 23, 24, 25]. To guarantee that the responses measured with CBC are identical to the open-loop responses measured with a single-harmonic voltage input to the shaker, a so-called non-invasiveness condition resulting in the cancellation of the higher-harmonics in the control signal has to be satisfied [24, 26]. CBC has been applied to cantilever beams with magnetic or geometric nonlinearities exhibiting bifurcation points and multiple branches of responses. It has been used to identify FRCs [22, 20], back-

bone curves [25] and bifurcation curve [27]. As FRCs cannot be parametrized uniquely by the response amplitude or frequency, their identification using CBC necessitates continuation algorithms such as the pseudo-arclength method [22]. An easier alternative is to find a parametrization of the response surface that does not require such algorithms. Exploiting the fact that CBC uses a response-based feedback controller, the response surface can be easily characterised by collecting responses at constant forcing frequency Ω (yellow curve in Fig. 1a). These curves, called S-curves due to their usual shape, are characterized by a monotonous evolution of the response amplitude and can be interpolated to extract FRCs [24, 18].

Another experimental method relies on feedback control using a phase-locked loop (PLL) to impose the phase lag between excitation and response of nonlinear systems [28, 29]. Fig. 1b shows that the phase lag and excitation amplitude fully parametrize the surface, rendering unnecessary the use of complicated continuation methods to identify FRCs. FRCs at constant excitation amplitude can be identified straightforwardly by imposing the phase lag [28, 30]. Backbone curves can also be identified by imposing phase quadrature, linking directly the method to the identification of NNMs. PLL testing has been successfully applied for the characterization of NNMs in many experiments including a blade [31] and a joint [32] with frictional nonlinearities, a circular plate [19] exhibiting hardening and modal interaction, and a cantilever beam with magnetic nonlinearity [33].

Response-controlled stepped-sine testing (RCT) is similar in principle to CBC as the control law is used to impose a particular response to the system, permitting the identification of constant-response FRFs [34], shown in a dashed purple curve in Fig. 1a. By imposing a constant response amplitude rather than a constant excitation amplitude, constant-response FRFs do not exhibit bifurcation points, even if the FRCs exhibit one or multiple turning points. A collection of constant-response FRFs can be identified to interpolate the surface and extract FRCs. RCT has been used, notably on a satellite structure [34], on a T-beam, on a guided missile and its control fin [35, 36].

These control-based methods measure directly the features of interest: Identifying the frequency response of the structure or the backbone of a nonlinear mode is invaluable in the industry e.g. for rapid prototyping. Such a characterization of nonlinear systems can be used for system stabilization [37] or vibration mitigation through nonlinear control [38]. For some systems, physics-driven modelling is still not predictive enough e.g. frictional systems with uncertainties or bolted joints [39]. Data-driven modelling is an attractive and attainable alternative.

The objective of this article is to present and compare control-based testing techniques in a theoretical and practical point of view, and to apply them on the same structure for the first time. The control laws used for RCT have not been disclosed (e.g. proprietary software was used in [35]). For this reason,

this article focuses specifically on PLL testing and CBC. The test rig and its design are presented in Section 2. Section 3 explains the two methods and discusses their main differences. Experimental data obtained successively with PLL testing and CBC is presented in Section 4. A detailed comparison between FRCs and backbone curves obtained with both methods is made. Conclusions are presented in Section 5.

2 Design and linear modal analysis of the test rig

The main structure of the experimental campaign consists of a thin arched beam whose both ends are clamped via bolted joints to a frame. The beam is specifically designed with a slight curvature in order to observe a softening-hardening behavior in the experiments. Unlike the flat beams, the stiffness of curved structures first decreases while the onset of buckling approaches, then it starts to increase after a certain point due to large deformations resulting in axial-bending stretches [40]. The difference between the dynamics of flat and curved beams is experimentally shown with a comparison study in [41]. Moreover, arched beams have also sophisticated characteristics that increase the complexity of the systems [42, 43]. All of these phenomena challenge the methods for the identification of the beam's dynamic features and enable a thorough comparison with their positive and negative aspects on a difficult system.

The beam's shape is defined as a circular arc with radius of curvature R and constant thickness h, see Fig. 3. The objective of the design was to select a combination of R and h such that the beam's first bending mode exhibits a pronounced softening-hardening behavior qualitatively similar to the one exhibited by system (1) without snap-through phenomenon (to avoid chaotic motions) nor internal resonances in the amplitude range of interest. To this end, we performed a preliminary parameter study of a finite element model of the ideally clamped arc with respect to R and h. More specifically, a reduced order model (ROM) of the finite element model was created to confirm that the system follows the desired dynamics using the implicit condensation procedure (see e.g. [44] for details about the method) and is used as the introductory example (1). The ROM was exposed independently to both static point load at center as well as dynamic excitation. In the latter case, the clamping points were moved harmonically in the vertical direction where both nonlinear normal modes (NNMs) and FRCs corresponding to the lowest frequency bending mode were computed using the free tool NLvib [45]. The nominal numeric values for R and h resulting from this study are given in Fig. 3.

The arched beam was manufactured by wire electrical discharge machining

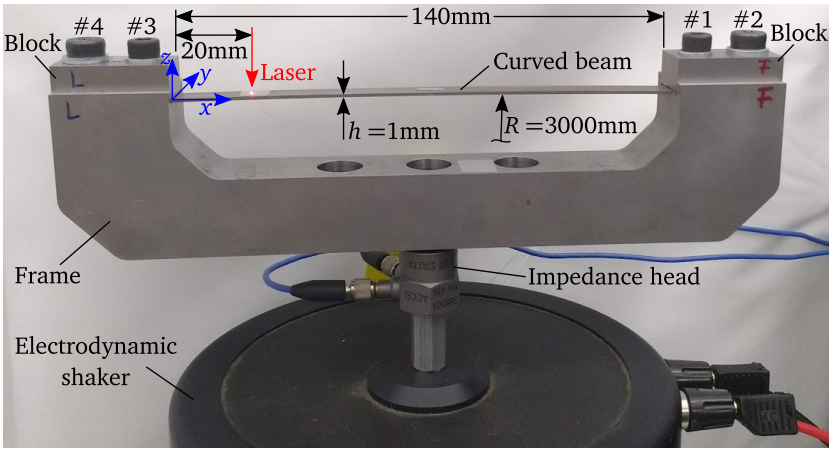

Figure 3: Test rig consisting in a thin arched beam with both ends clamped to a frame which is connected to an electrodynamic shaker

using spring steel 1.8159 (density 7.7-8.03 $\times$ 1000 kg/m^3, Poisson's ratio 0.27-0.30, Young's modulus 190-210 GPa). To ensure the clamped-clamped boundary conditions, a stiff support frame and two identical clamping blocks were designed and manufactured from the same steel as the beam to avoid stresses as a consequence of temperature change. On both sides (left and right), the beam's ends are laid between the frame and a block, after which the block is clamped via two screws toward the frame. The outer screws (#2 and #4) are fitting screws ISO 7379 which are tightened by hand and have the function to uniquely define the longitudinal position of the blocks. On the right-hand side, #2 also positions the beam longitudinally, whereas on the left-hand side the bore through the beam's end has a bigger diameter than the fitting screw such that axial prestress in the beam are avoided. #1 and #3 are M5x25 hexagon socket screws with the function to generate a contact pressure large enough to avoid macroslip of the beam's ends in the joints during vibration tests. Therefore they are fixed by a defined torque of 6 Nm. To avoid as much variation as possible in the axial prestress caused by the bolts, the order of tightening the screws is defined by #1 $\rightarrow$ #2 $\rightarrow$ #3 $\rightarrow$ #4. The resulting curvature of the beam in its clamped-clamped configuration may differ from the nominal shape as a consequence of imperfections of manufacturing and assembly processes. The actual surface profile of the beam in its clamped configuration is measured by means of the height of the top surface using a laser scanner (Keyence LK-H052), see Fig. 4. The height increases significantly and in a symmetrical manner from left and right sides toward center as intended. The rectangles with increased height close to the left clamping point and at center are reflection tapes which were glued at these positions. The final geometry is very close to the nominal profile.

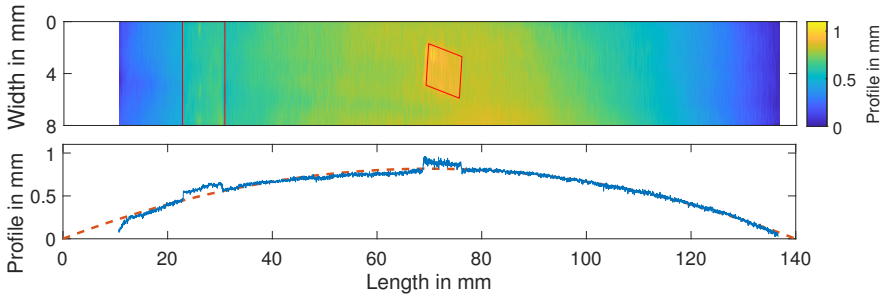

Figure 4: Top: height surface profile of the beam's top face, reflective tape highlighted in red; bottom: mid-width profile (plain blue curve) and nominal profile (dashed orange curve)

The frame supporting the curved beam is connected to an electrodynamic shaker (B&K type 4809 driven by amplifier type 2718). An impedance head (PCB 288D01) is placed between the shaker's armature and the frame to measure both excitation force and acceleration of the frame at the drive point. The beam's response is measured by a laser Doppler vibrometer (Polytec OFV-5000 with OFV-552-2 laser head) 20 mm away from the left clamping. The measurement location was chosen close to clamping to avoid instabilities in feedback loops emanating from the measurement and driving points being non-collocated.

The velocity v measured by the laser vibrometer constitutes the beam's response and the force f measured by the impedance head constitutes the excitation. When a harmonic voltage of the form $u(t) = U\sin(\Omega t)$ is sent to the electrodynamic shaker, it generates the force $f(t)$. If the response is periodic, it can be approximated by a truncated Fourier series of N harmonics

$$v(t) = \sum_{n=1}^{N} \hat{\alpha}_{v,n} \sin(n\Omega t) + \hat{\beta}_{v,n} \cos(n\Omega t). \tag{2}$$

In practice, only a limited number of harmonics is considered. Subharmonic components of the form

$$\hat{\alpha}_{v,n/\nu} \sin\left(\frac{n}{\nu}\Omega t\right) + \hat{\beta}_{v,n/\nu} \cos\left(\frac{n}{\nu}\Omega t\right), \quad \frac{n}{\nu} \notin \mathbb{N} \tag{3}$$

are not taken into account in this study because their amplitudes was negligible in the experiments described in the rest of the article. The fundamental amplitude of the response is defined as $V_1 = \sqrt{\hat{\alpha}_{v,1}^2 + \hat{\beta}_{v,1}^2}$ and the fundamental phase lag $\phi_v = \operatorname{atan2}(\hat{\beta}_{v,1}, \hat{\alpha}_{v,1})$. The phase lag defined on the velocity causes the the periodic responses to be in phase quadrature—or in phase resonance—when $\phi_v = 0$ rad.

At low forcing amplitudes, the beam is assumed to behave linearly. Therefore, the modal properties corresponding to the lowest frequency bending mode

of the underlying linear system are determined using a hardware platform for linear modal analysis (m+p VibRunner). A random voltage signal was sent to the shaker's amplifier with an amplitude of 0.03 V and a frequency range between 10 and 3200 Hz. The natural frequency has been measured to be $\omega_0 = 1988$ rad/s, and the damping ratio $\delta_0 = 0.026\%$. The mode shape of the experiment is not to be confused with the beam's (continuous) deflection shape. Rather, it is defined by the relationship between the acceleration of the base and the velocity of the beam at the measurement point. To realize the control loops of PLL testing and CBC (see Sect. 3.1 and 3.2 for details), the sensors and the amplifier are connected to a rapid control prototyping system (dSPACE MicroLabBox, sampling frequency: 10,000 Hz).

3 Methods

Phase-locked loop (PLL) testing and control-based continuation (CBC) are introduced in Sections 3.1 and 3.2 respectively. Continuation algorithms to identify backbone curves and FRCs are developed in Sections 3.3 and 3.4 respectively. Section 3.5 focuses on a method to compensate for shaker-structure interaction and recover a single-harmonic input force. PLL testing and CBC are compared from a theoretical point of view in Section 3.7. A comparison based on experimental results will be given in Section 4.

3.1 Phase-Locked Loop testing

The basic working principle of PLL testing is illustrated in Fig. 5. A sine signal

$$u(t) = U \sin(\theta(t)) = U \sin\left(\int_0^t \Omega(\tau)\,\mathrm{d}\tau\right), \tag{4}$$

with instantaneous phase $\theta(t)$ and time-varying excitation frequency $\Omega(t)$ is provided as voltage input to the experimental set-up. The excitation frequency Ω is calculated by a PID control law,

$$\Omega(t) = \omega_0 + k_\mathrm{p}(\phi_\mathrm{ref} - \phi_v(t)) + k_\mathrm{i}\int_0^t (\phi_\mathrm{ref} - \phi_v(\tau))\,\mathrm{d}\tau - k_\mathrm{d}\frac{\mathrm{d}\phi_v}{\mathrm{d}t}(t), \tag{5}$$

aiming at reaching a reference phase lag ϕ_ref between the fundamental harmonic of the excitation f and response x [28]. When the controller has settled, i.e. when the excitation frequency remains constant, the voltage signal is monoharmonic.

A key task within PLL testing is to evaluate the phase lag ϕ_v online, i.e. at each time sample of the experiment. One method to perform this is the

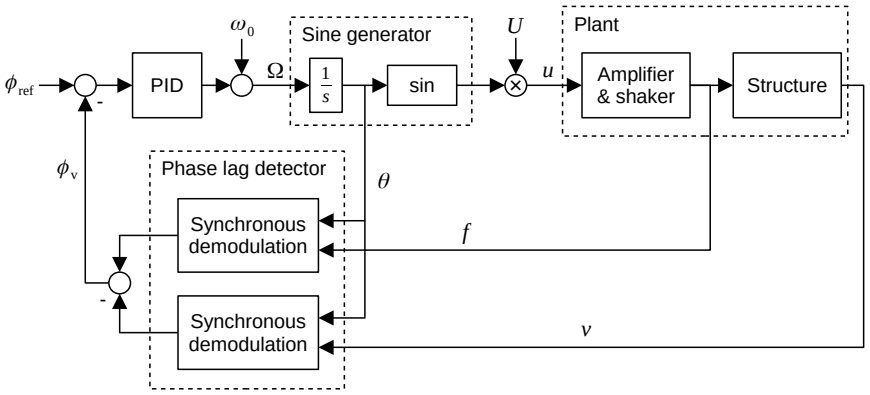

(a)

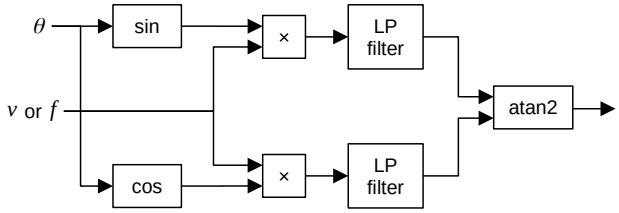

(b)

Figure 5: (a) Phase-Locked Loop and (b) synchronous demodulation [46]

synchronous demodulation shown in Fig. 5b that consists in an online Fourier decomposition using linear low-pass (LP) filters. It has been successfully applied in other PLL tests [29, 33, 30, 19] and is used in this work. A promising alternative is the use of adaptive filters [26] to perform the online Fourier decomposition.

PLL has been shown capable of stabilizing unstable orbits depending on the gains of its controller [19]. The tuning of the gains is discussed in Section 3.6. The time constant of the low-pass filter used for phase demodulation is 0.4 s. This values was selected to compromise between convergence time and filtering capacity.

3.2 Control-Based Continuation

The general formulation of CBC, as presented in [16], separates the excitation from the control signal that can be applied along the excitation by the same

actuator or by a separate actuator. The present article exploits a simplified implementation of CBC [24] shown in Fig. 6, in which the excitation is provided by the controller.

The voltage signal u is generated by a PD controller whose input is the difference between a reference signal y and the velocity v measured by the laser vibrometer:

$$u(t) = k_\mathrm{p}(y(t) - v(t)) + k_\mathrm{d}\frac{\mathrm{d}}{\mathrm{d}t}(y(t) - v(t)). \tag{6}$$

The PD controller modifies how the system responds to perturbation and can stabilize unstable orbits [47]. The tuning of the control gains are discussed in Section 3.6. Note that CBC does not require a specific type of controller such that other control law could have been used.

The multi-harmonic response of the system generally leads to a multi-harmonic control signal. At steady state, the response (Eq. (2)) and the input voltage signal can be approximated with truncated Fourier series of N harmonics:

$$u(t) = \sum_{n=1}^{N} \hat{\alpha}_{u,n}\sin(n\Omega t) + \hat{\beta}_{u,n}\cos(n\Omega t). \tag{7}$$

There exist multiple methods to perform the Fourier decomposition. Offline methods need to gather data during one or more periods before computing the coefficients, as such they work at a frequency lower than the controller. Online methods update the coefficients at every sample time or at the same frequency than the controller. Both are compatible with CBC [26]. In this article, the decomposition is performed offline by integrating one period of the signal following Fig. 6b. The reference signal is constructed to be multi-harmonic with its fundamental component

$$y_\mathrm{f}(t) = \hat{\alpha}_{y,1}\sin(\Omega t) + \hat{\beta}_{y,1}\cos(\Omega t) \tag{8}$$

and non-fundamental component

$$y_\mathrm{nf}(t) = \sum_{n=2}^{N} \hat{\alpha}_{y,n}\sin(n\Omega t) + \hat{\beta}_{y,v}\cos(n\Omega t). \tag{9}$$

To compare CBC with PLL testing or even standard open-loop testing methods such as stepped sines, it is necessary to recover a monoharmonic input voltage signal, i.e. $(\hat{\alpha}_{u,n}, \hat{\beta}_{u,n})_{n=2}^{N} = 0$. This can be achieved by adequately choosing the higher-harmonics of the reference signal. Eq. (6) shows directly that u is monoharmonic when

$$(\hat{\alpha}_{y,n}, \hat{\beta}_{y,n})_{n=2}^{N} = (\hat{\alpha}_{v,n}, \hat{\beta}_{v,n})_{n=2}^{N}. \tag{10}$$

Eq 10 is a zero problem that can be solved using standard root-finding methods while the physical experiment is running. The solver can operate at a frequency

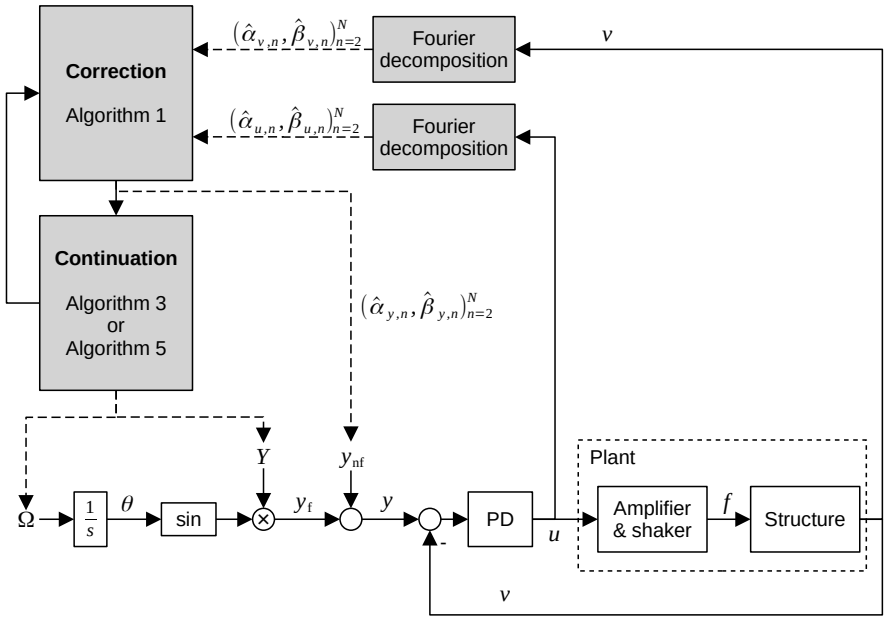

(a)

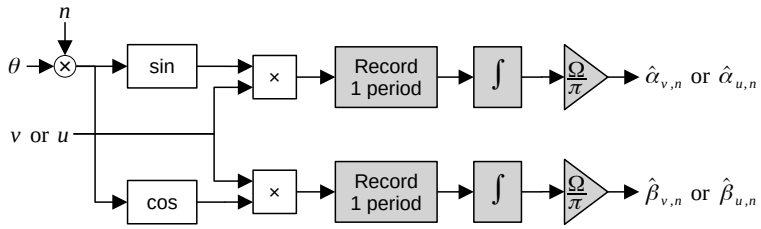

(b)

Figure 6: (a) Control-Based Continuation consisting in an online feedback loop and offline correction/continuation algorithms, (b) offline Fourier decomposition for harmonic n; offline operations are displayed as grey boxes

Table 1: Parameters for Algorithm 1

Y_{init} in m/s	t_{wait} in s	N	tol in V
0.01	1	3	0.05

that is different or identical to the real-time controller, making iterations offline or online [26] respectively. In this article, the algorithm runs offline and consists in derivative-free Picard-iterations [24]. It is presented in Algorithm 1 and its parameters are shown in Table 1. For the rest of the article, the left arrow operator ($\cdot \leftarrow \cdot$) signifies a value assignment.

Algorithm 1 Algorithm to make the voltage monoharmonic during CBC

1: $(\hat{\alpha}_{y,1}, \hat{\beta}_{y,1}) \leftarrow (Y_{\text{init}}, 0)$
2: **repeat**
3: Wait a duration t_{wait} for steady state
4: Record time series u and v during one period
5: Perform Fourier decomposition on u and v
6: $(\hat{\alpha}_{y,n}, \hat{\beta}_{y,n})_{n=2}^{N} \leftarrow (\hat{\alpha}_{v,n}, \hat{\beta}_{v,n})_{n=2}^{N}$
7: **until** $\max_n \left((|\hat{\alpha}_{u,n}|, |\hat{\beta}_{u,n}|)_{n=2}^{N} \right) < \text{tol}$

The phase of the reference signal can be constrained by setting $\hat{\beta}_{y,1} = 0$. The only two adjustable parameters of the experiment are the frequency of excitation Ω and the fundamental reference amplitude $Y = \hat{\alpha}_{y,1}$. The excitation amplitude F is not defined by the user but depends on the response v and reference amplitude Y. Furthermore and contrarily to PLL, measuring the excitation f is not necessary for the method but is only an output of the experiment.

3.3 Identification of backbone curves

Phase quadrature is directly imposed by the PLL to identify responses of the backbone curve. A sequential continuation (i.e. a parameter stepping) shown in Algorithm 2 is followed to step through different amplitude levels. Its parameters are shown in Table 2. For the rest of the article, simple loops are used in algorithms to signify that the interruption is at the user's discretion. For the identification of backbones, it is practical to start at low amplitude and use the corresponding natural frequency ω_0 of the underlying linear system as initial condition for the resonance frequency ω [32].

Keeping the reference amplitude Y constant during CBC and varying the excitation frequency Ω allows the continuation of periodic responses with an indirect constraint on the response amplitude under which a single periodic re-

Algorithm 2 Algorithm to identify backbone curves during PLL testing

$\phi_{\mathrm{ref}} \leftarrow 0$
$U \leftarrow U_{\mathrm{init}}$
loop
  Wait for convergence of Ω
  Save response
  $U \leftarrow U + \Delta U$
end loop

Table 2: Parameters for Algorithm 2

U_{init} in V	ΔU in V
0.006	0.006

sponse is in phase resonance (similar to constant-response FRFs). CBC therefore enables the identification of backbone curves by performing a sequential continuation on Y and solving $\phi_v(\Omega) = 0$ at every step using the bisection method, as was done in [25]. Both are implemented in Algorithm 3 with parameters shown in Table 3.

Algorithm 3 Algorithm to identify backbone curves during CBC

$Y \leftarrow Y_{\mathrm{init}}$
$\Omega \leftarrow \omega_0$
loop
  $\Delta\Omega \leftarrow \Delta\Omega_{\mathrm{init}}$
  Make voltage monoharmonic following Algorithm 1
  Evaluate ϕ_v
  while $|\phi_v| > \mathrm{tol}_\phi$ **and** $|\Delta\Omega| > \mathrm{tol}_\Omega$ **do**
    if $\mathrm{sign}(\phi_v\, \Delta\Omega) < 0$ **then**
      $\Delta\Omega \leftarrow -\Delta\Omega/2$
    end if
    $\Omega \leftarrow \Omega + \Delta\Omega$
    Make voltage monoharmonic following Algorithm 1
    Evaluate ϕ_v
  end while
  Save response
  $Y \leftarrow Y + \Delta Y$
end loop

In summary, the same phase quadrature can be attained by different means during PLL testing and CBC. On the one hand, PLL testing is an online method in that the phase lag converges continuously towards quadrature thanks to the PID controller acting on the excitation frequency. On the other hand, CBC is

Table 3: Parameters for Algorithm 3

Y_{init} in m/s	$\Delta\Omega_{\text{init}}$ in rad/s	tol_ϕ in rad	tol_Ω in rad/s	ΔY in m/s
0.01	1	0.05	0.01	0.02

an offline method, i.e. successive periodic responses are identified and an algorithm is used to iterate automatically the excitation frequency until quadrature is found up to tolerance. More operations are made online during PLL testing (numerical integration, synchronous demodulation) while CBC's offline continuation algorithm possesses more steps. The amplitude of the periodic responses are determined by the voltage signal U, defined directly during PLL testing or indirectly through the reference amplitude Y during CBC.

Limitations of the algorithms presented in this section arise when confronted to internal resonance. In such a case, both the excitation amplitude and the fundamental response amplitude are expected to locally decrease along the backbone curve [48]. Given that Algorithm 2 increases the excitation amplitude sequentially and that Algorithm 3 increases the fundamental reference amplitude sequentially, such drop would result in a jump in the backbone curve. More complex continuation algorithms using, for instance, pseudo-arclength continuation would be required to characterize fully such systems.

3.4 Identification of FRCs

The identification of FRCs requires a constant-amplitude, usually single-harmonic excitation. To reach a constant excitation amplitude F at the fundamental excitation frequency, the feedback loop shown in Fig. 7 is introduced on top of the controlled experiment. This loop contains a synchronous demodulation to measure F online and a PID controller that adjusts the amplitude U of the voltage signal to reach the forcing amplitude F_{ref}. The force applied to a nonlinear structure also contains higher harmonics, which typically result from shaker-structure interactions and the lack of linearity between the voltage sent to the shaker's amplifier and the force applied by the shaker. A method to compensate for these higher harmonics and cancel them is presented in Section 3.5.

The algorithm to identify FRCs using PLL testing is shown in Algorithm 4. It performs a sequential continuation on the phase lag in the vicinity of the resonance [30]. For lightly damped structures, the ratio $\partial\Omega/\partial\phi$ is small at resonance but large away from it. To avoid divergence of the controller after a phase step (e.g. towards another mode) and to obtain reasonably spaced data points in the amplitude frequency plane, smaller steps of the reference phase are chosen away from resonance as shown in Fig. 8.

Although CBC can be used for the direct identification of FRCs, more

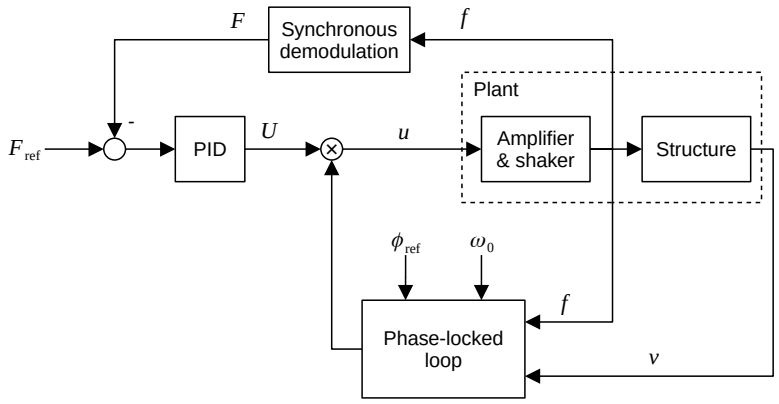

Figure 7: Amplitude control of the voltage U to reach a reference excitation amplitude F_{ref} for the identification of FRCs during PLL testing

Algorithm 4 Algorithm to identify FRCs during PLL testing

1: F_{ref} defined by user
2: $\phi_{\mathrm{ref}} \leftarrow \phi_{\mathrm{init}}$
3: **loop**
4: Wait for convergence of U and Ω
5: Save response
6: $\phi_{\mathrm{ref}} \leftarrow \phi_{\mathrm{ref}} + \Delta\phi$
7: **end loop**

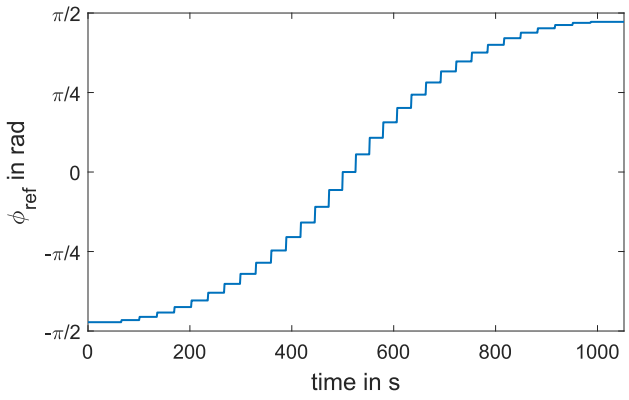

Figure 8: Time profile of ϕ_{ref} for Algorithm 4

Table 4: Parameters for Algorithm 5

Y_{init} in m/s	Ω_{init} in rad/s	ΔY in m/s	$\Delta\Omega$ in rad/s
0.01	1967	0.01	3.14

complicated continuation procedures are required to go around fold bifurcations [22, 20, 49]. It is usually easier to identify S-curves and extract FRCs through post-processing as in [25]. Keeping the excitation frequency Ω constant and varying Y enables the continuation of S-curves following Algorithm 5, with its parameters shown in Table 4. In the absence of internal resonance, S-curves vary monotonically with Y and a sequential continuation procedure is applicable. Identifying a collection of S-curves at different frequencies and defining a suitable interpolation allows to identify the full (continuous) response surface. Regression techniques can then be exploited to approximate FRCs at constant excitation amplitude F. This indirect identification removes therefore the need for the feedback loop applied to the fundamental excitation amplitude shown in Fig. 7 and used during PLL testing.

Algorithm 5 Algorithm to identify a collection of S-curves during CBC in order to approximate FRCs from the dynamic response surface

$Y \leftarrow Y_{\text{init}}$
$\Omega \leftarrow \Omega_{\text{init}}$
loop
  loop
    Make voltage monoharmonic following Algorithm 1
    Save response
    $Y \leftarrow Y + \Delta Y$
  end loop
  $Y \leftarrow Y_{\text{init}}$
  $\Omega \leftarrow \Omega + \Delta\Omega$
end loop

In summary, the same periodic responses can be identified during PLL testing and CBC. In the former, an arbitrary phase lag is imposed thanks to the PLL. However, it is necessary to add an additional control loop during PLL testing in order to impose a desired excitation amplitude F and identify FRCs. CBC can identify FRCs directly and would, in that case, also require such a control loop on the excitation. Alternatively, S-curves can be identified sequentially and interpolated into a continuous response surface in post-processing, providing an approximation of the FRCs of interest. As discussed in Section 3.5, the two methods require an additional control loop to cancel higher harmonics present in the applied excitation (if desired).

3.5 Compensation of the shaker-structure interaction

Shaker-structure interaction (SSI) can result in multiple phenomena including resonance force drop, jumps, internal resonance, or subharmonic resonance [50]. Although these phenomena were not observed in the experiments of this article, higher harmonics in the applied force were. As the excitation is directly measured at the application point by an impedance head, it can be directly validated: If the force signal is close to a sine wave at the desired amplitude, the system's response is accepted.

Without additional control, a monoharmonic voltage u can lead to a multiharmonic excitation f [32]. The excitation f can be approximated by a truncated Fourier series of N harmonics:

$$f(t) = \sum_{n=1}^{N} \hat{\alpha}_{f,n} \sin(n\Omega t) + \hat{\beta}_{f,n} \cos(n\Omega t). \tag{11}$$

The amplitude and phase of harmonic n are expressed as $F_n = \sqrt{\hat{\alpha}_{f,n}^2 + \hat{\beta}_{f,n}^2}$ and $\phi_{f,n} = \operatorname{atan2}(\hat{\beta}_{f,n}, \hat{\alpha}_{f,n})$, respectively. Once the voltage u is monoharmonic during CBC or PLL testing, a correction is computed from its instantaneous voltage phase θ by a proportional controller:

$$u_{\mathrm{nf},n} = -k_{\mathrm{p}} F_n \cos\left(n\theta(t) - \phi_{f,n}\right) \tag{12}$$

shown in Fig. 9. In this paper, this correction was done for only $n = 2$ and 3 as the higher harmonics were not significant in the experiments. The controller gain is discussed in Section 3.6.

This method makes the assumption that the shaker is phase-neutral, i.e. the phase-lag between the voltage and the force is zero. At high amplitudes, when the SSI is most significant, the shaker indeed approaches phase-neutrality and the higher harmonics are reduced by the feedback loop. At low amplitudes, the phase-lag added by the shaker approaches 90° between the voltage and the force. The violation of the assumption is considered acceptable due to the low amplitude of higher harmonics in this case. The limitations of the method are considered out of this article's scope. Until more analytical work is done, the method is to be considered *ad-hoc* and not generally applicable.

Fig. 10 shows the amplitude of the first four harmonics of the excitation signal f for resonant periodic responses experimentally measured at different response amplitudes. Without SSI compensation, the excitation signal is clearly multiharmonic. After closing the SSI compensation control loop, the higher harmonics are significantly reduced. Interestingly, a slight variation in fundamental excitation amplitude is noted as well, showing the influence of higher excitation harmonics on the periodic response.

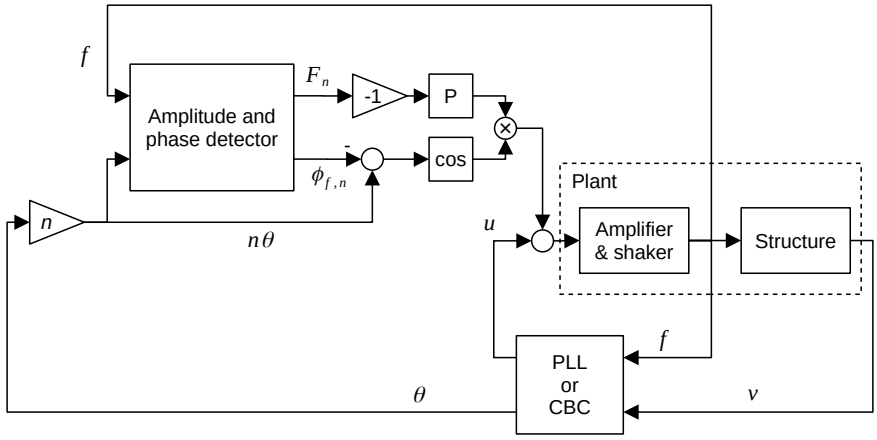

Figure 9: Shaker-structure interaction control correcting the n^{th} harmonic of the voltage by a proportional controller (P)

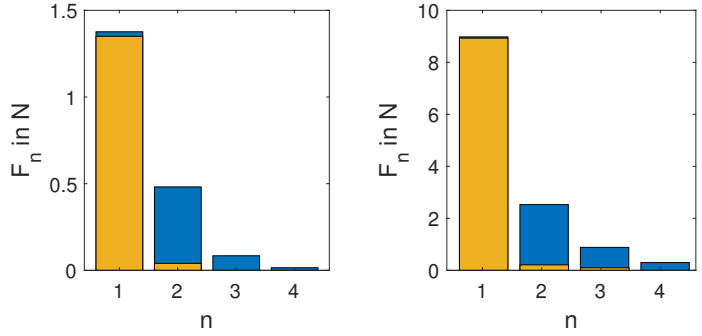

(a) (b)

Figure 10: Frequency content of the resonant force signal at amplitudes (a) $V_1/(\Omega h) \approx 0.1$ and (b) $V_1/(\Omega h) \approx 0.25$ with and without shaker-structure interaction control (yellow and blue, respectively)

3.6 Controller gains

There is currently no general method to construct a control law for control-based methods to reach their control objectives—e.g. the stabilization of unstable responses—without knowing some characteristics of the system. However, control-based methods are meant to be applicable without the need to identify a model beforehand. There is some promising but very early proposals for such tuning methods, for instance using control Lyapunov-Razumikhin functions [51] or adaptive control design [52]. In the meantime, control gains are tuned heuristically, i.e. by trial and error. The scope of this article is not to derive formally the influence and effect of each control gain on the dynamics of general systems. Rather, this Section presents guides to tune the controllers for PLL testing and CBC.

The controller used during PLL testing has a conventional purpose: A measured value must converge towards a setpoint. Specifically for PLL testing, the phase lag ϕ_{v} between the beam's velocity and the force detected by synchronous demodulation must converge towards the reference phase lag ϕ_{ref}. One can therefore use manual tuning for PID controllers, as proposed for instance in [53], showing that the time needed to converge towards the target depends heavily on the controller gains. The PID gains found in this way are shown in the first column in Table 5. A similar methodology is used for tuning the PID controller used to impose a constant force amplitude. The gains are shown in the third column of Table 5.

The feedback control used in the simplified CBC method steers the response of the system towards a setpoint but it is not meant to reach it. The main purpose of the controller is to stabilise the unstable response of the uncontrolled system. Velocity feedback modifies the effective damping of the structure while displacement feedback modifies its effective stiffness [54]. Adding or removing effective damping reduces or increases the transient time respectively. In this article, the signal fed back is directly the velocity. The PD controller includes a proportional gain adjusting the velocity feedback and a differential gain adjusting the acceleration feedback (analog to a displacement feedback). Practically, a frequency at which the structure exhibits unstable responses at the force levels of interest is chosen. Successive S-curves are identified using CBC, increasing progressively the controller gains until all of the S-curve is stabilized. The corresponding gains of the PD controller are shown in the second column of Table 5.

3.7 Comparison of the methods

To summarize the previous sections, a general comparison of the working principles behind phase-locked loop (PLL) testing and control-based continuation

Table 5: Gains of the controllers used in PLL testing and in CBC (* backbone identification, † FRC identification)

	PLL		Ampl. control (PLL)		CBC		SSI control
k_p	150	s^{-1}	$120^\dagger$		20	Ns/m	12^*,$40^\dagger$
k_i	50	s^{-2}	$40^\dagger$	s^{-1}	–		–
k_d	40^*, $10^\dagger$		$0.04^\dagger$	s	0.4	Ns^2/m	–

(CBC) is summarized below.

Control	**PLL testing** includes a controller designed to reach a phase lag target. It is usually a PI controller [29], the proportional gain providing stability and the integral gain leading to a zero set point error. The control and excitation are applied via the same actuator. **CBC** includes a controller designed to stabilize the system's response by comparing it to a reference signal. The actuator used to apply the control can be identical or different to the one used to apply the system excitation. With the simplified CBC method, the controller is not required to reach the reference signal. Examples of controllers include PD controllers [16] and controllers designed by pole-placement techniques [18].
Identified features	**PLL testing** controls the phase lag: It is naturally suited to identify backbone curves [29] and FRCs [28, 30]. **CBC** controls the response signal: It can identify FRCs [24, 22, 20] and backbone curves [25] but can also reach a broader range of responses that might not be well parametrized by the phase [27].
Harmonic excitation	**PLL testing** is designed to send a monoharmonic voltage to the exciter once the PLL has converged, such that measured responses are directly comparable with responses obtained with open-loop methods such as stepped sines. With **CBC**, the voltage provided to the exciter is a priori multi-harmonic such that a specific reference signal must be found to recover results comparable with open-loop tests. **Both methods** require additional control loops to cancel higher harmonics present in the applied force.
Online/offline variants	**PLL testing** is an online method, i.e. the method runs in real time. The Fourier decomposition must be online as the phase lag is fed to the controller. **CBC** comprises in general an offline algorithm running in parallel to the experiment and performing the continuation procedure. Online variants are possible [26].

Additionally, here is a comparison of more practical aspects focusing on the continuation algorithms to identify FRCs and backbone curves, the features of interest in this article.

Identification of backbone curves	With **PLL testing**, backbone curves are identified by keeping the phase lag constantly at quadrature and performing a sequential continuation on the voltage amplitude. With **CBC**, backbone curves are identified by performing a sequential continuation on the voltage amplitude and finding phase quadrature at each step by iterating on the excitation frequency.
Identification of FRCs	With **PLL testing**, FRCs are identified by keeping the force amplitude constant via an additional control loop and performing a sequential continuation on the phase lag. With **CBC**, FRCs can be identified by implementing a pseudo-arclength continuation [22]. In this article, FRCs are extracted from a collection of S-curves identified by keeping the frequency constant and performing a sequential continuation on the voltage amplitude.

4 Experimental results

The system is subjected to a series of experiments to characterize the first bending mode of the beam. Specifically, a harmonic force $f = F\sin(\Omega t)$ is applied vertically to the frame. Its acceleration a is measured by the impedance head while the velocity v of the beam is measured by the laser vibrometer. When periodic, these signals define closed orbits characterizing the system's response to the excitation.

PLL testing and CBC are independently used to identify the periodic responses of the beam at and around the resonance of the first bending mode. The excitation frequency at resonance ω depends on the amplitude of the response and is obtained through the identification of backbone curves in Section 4.1 following the method presented in Section 3.3. The backbone is used for estimating the modal properties of the NNM, presented in Section 4.2. These properties define a reduced order model which enables to synthesize FRCs in the vicinity of the mode, presented in Section 4.3. Additionally, FRCs are directly identified during experiments in Section 4.4 following the method presented in Section 3.4.

4.1 Backbone curves

Figure 11a shows backbone curves identified during PLL testing and CBC following Algorithms 2 and 3 respectively. The experiment was repeated six times

in a row with each method to assess repeatability. The first experiment of the series applied CBC and resulted in a qualitatively different identification (dashed curve). It is suspected that the temperature of the beam increased during the experiment, resulting in a change of modal properties. The curve is therefore discarded while the five subsequent CBC experiments and six PLL testing experiments constitute the results. The frequency content of two periodic responses—one at low amplitude in the softening regime and the other at high amplitude in the hardening regime—is shown in Figs. 11b and 11c. The low amplitude of higher harmonics relative to the fundamental supports the assumption that a single mode is excited without modal interaction.

The minimum amplitude reachable during the experiments depends on the signal-to-noise ratio. PLL testing requires an online Fourier decomposition for the phase lag to be fed into the PLL controller at each sample time. Low signal-to-noise ratio prevents the PLL to converge and thus low-amplitude responses to be identified. In contrast, the offline Fourier decomposition used during CBC can gather as much data as needed before proceeding with the continuation algorithm. This allows averaging of the signals and better performance at low signal-to-noise ratios.

The nonlinear natural frequency ω approaches the linear natural frequency ω_0 at low amplitudes using both methods. The beam exhibits a softening behavior until an amplitude $V_1/(\Omega h) \approx 0.15$ before which ω decreases with V_1. Above this amplitude, ω increases with V_1 in a hardening behavior. This turning point corresponds to a displacement amplitude of $0.67h$ at the beam's center (estimated using the linear mode shape of the FE model). A softening-hardening transition at this amplitude is expected from a slightly curved beam, as demonstrated in [55] showing excellent agreement between the results and theory.

Let the successive backbone curves be described by the functions $\omega_k(V_1)$ for the k^{th} curve. For every value V_1, the standard deviation $\sigma(\omega)$ is computed and shown in Fig. 12a. The standard deviation increases suddenly when reaching amplitude $V_1/(\Omega h) = 0.15$, corresponding to the softening-hardening transition, and stays large at higher amplitudes. The maximum standard deviation

$$\begin{aligned} \max_{V_1} \sigma(\omega_k(V_1)) &= 0.00145\omega_0 && \text{for PLL testing and} \\ &= 0.00137\omega_0 && \text{for CBC,} \end{aligned}$$

are comparable between the methods. These values are small in absolute value but relatively significant in the light of the amplitude-dependent frequency change of about -0.5 % and $+2$ % attributed to the softening and hardening behavior respectively. To adequately represent the repeatability variations, the standard deviation is included as colored areas next to the results in the rest of the article.

A potential explanation for this increase of variability with amplitude resides in the knowledge that steady state response of dry frictional systems under peri-

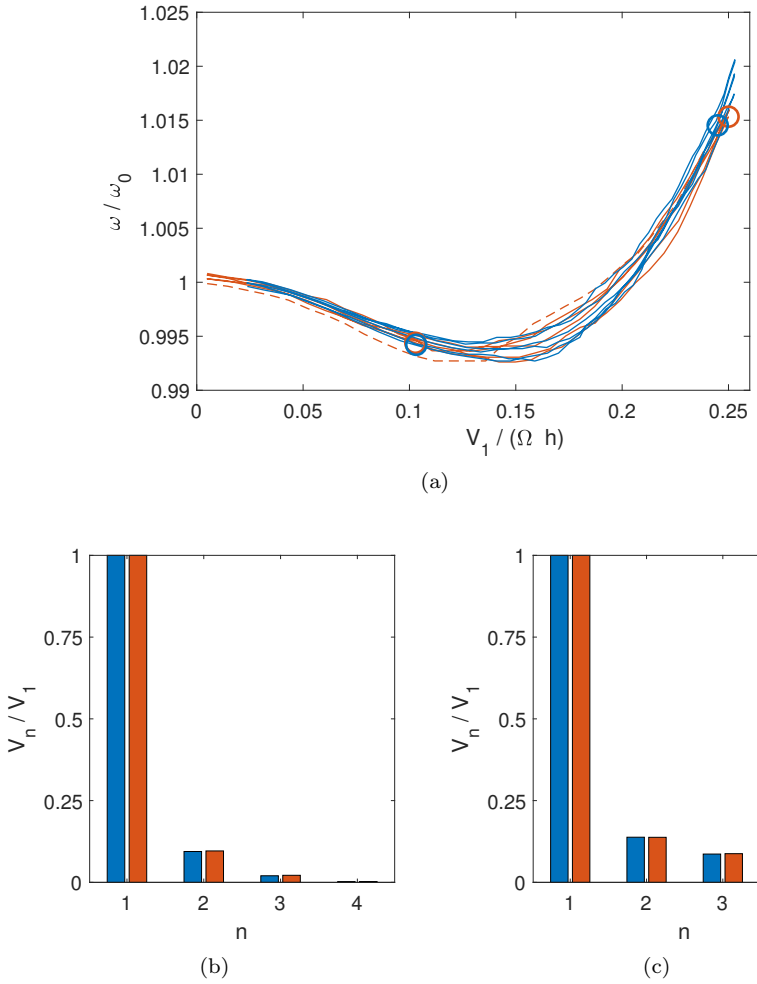

Figure 11: (a) Backbone curves identified with PLL testing (blue curve) and CBC (orange curve) from six successive experimental identifications (warm-up in dashed curve); frequency content of periodic responses at resonance and at amplitudes (b) $V_1/(\Omega h) \approx 0.1$ and (c) $V_1/(\Omega h) \approx 0.25$ identified during PLL testing (blue) and CBC (orange)

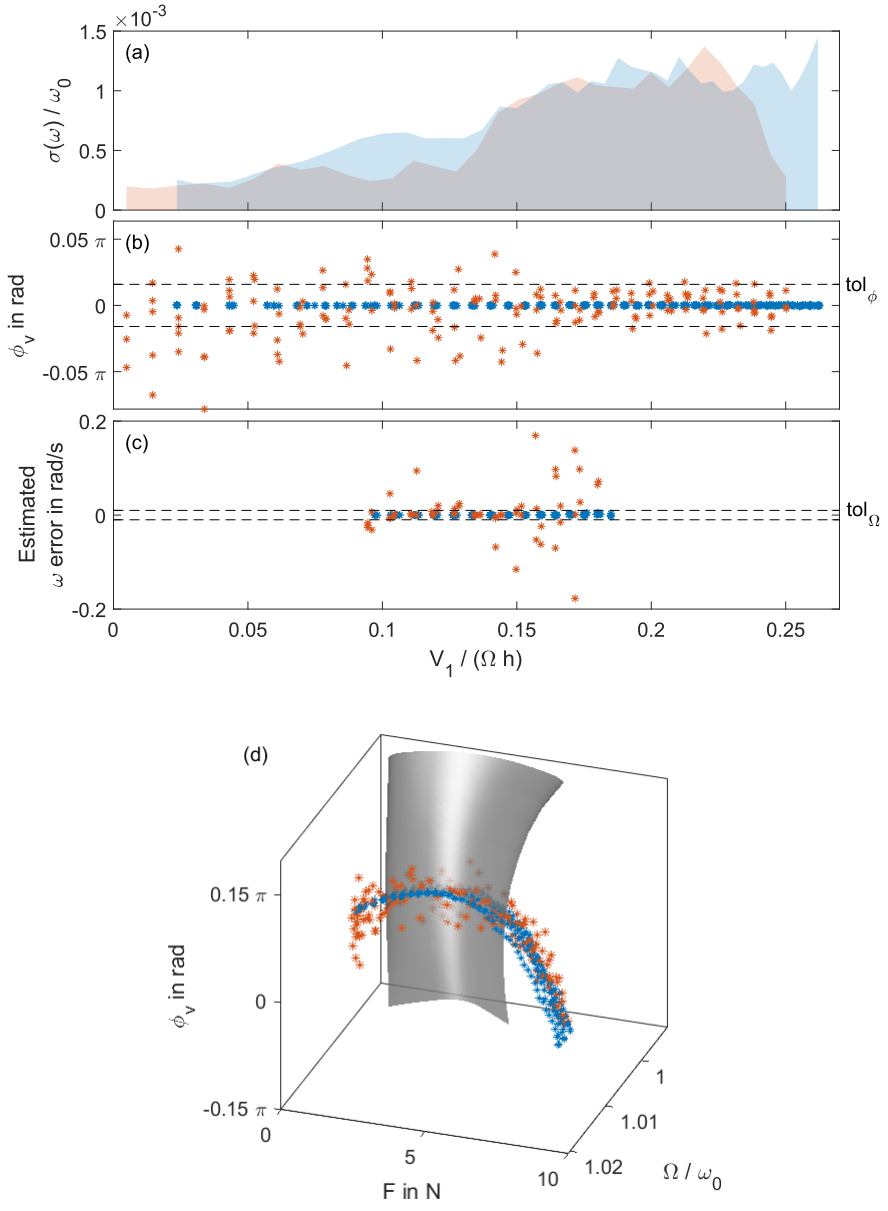

Figure 12: (a) Standard deviation of the successive backbone experiments using PLL testing (blue area) and CBC (orange area), (b) measured phase lag error and (c) frequency error in the identified backbone responses during PLL testing (blue curve) and CBC (orange line and squares) estimated from the (d) local response phase surface around the backbone

odic loading may depend on the initial conditions (slip displacements in sticking contact zones). These slip displacements can depend in a complex way on the entire load history of the system under consideration and are thus generally unknown. Consequently, repeated experiments can show a certain variability [39]. At small amplitudes, the contact area is mostly sticking, leading to a unique dynamic response. With increasing amplitude, the variability increases. In the macro-slip regime, theoretically, variability would decrease again, but this regime is not reached by bolted joints. This behavior is studied in detail for instance in [56].

Additionally, the softening effect characterized during the experiments and shown in Fig. 11a is much less pronounced than what is predicted from the numerical model (Fig. 1). The model assumes that the extremities of the beam are ideally clamped, whereas the actual joints are bolted. Predictive numerical models for bolted structures are extremely challenging to produce [39], highlighting the relevance of model-free control-based methods.

Fig. 12b shows the error in phase lag compared to the quadrature target $\phi_v = 0$ rad. PLL testing is able to reach a phase error almost two orders of magnitude lower than CBC. This is not surprising as CBC can only approach quadrature using prescribed finite steps, presently following Algorithm 3. Despite the higher precision achieved by PLL testing, the standard deviation shown in Fig. 12a is not reduced compared to CBC. It can be concluded that high phase precision is not needed in this particular application due to high inherent variability.

A frequency error shown in Fig. 12c is estimated as the distance from the local response surface shown in Fig. 12d. The surface is an interpolation of S-curves identified using CBC and presented later in the article (Fig. 16). Fig. 12b shows that most periodic responses identified during CBC at high amplitudes ($V_1/(\Omega h) > 0.15$) lie within the phase tolerance, while Fig. 12c shows that most periodic responses at low amplitudes ($V_1/(\Omega h) < 0.15$) lie within the frequency tolerance. This can be linked to later results showing that damping increases with amplitude (Fig. 13b). Lower damping implies a sharper resonance peak: The phase-lag is sensitive to small variations in frequency. As damping increases, the sensitivity to changes in frequency diminishes while the sensitivity to changes in phase-lag increases. The change in damping can be seen visually in Fig. 12d as the response surface is flatter on its left-hand boundary (lower amplitude and damping) and more curved on its right-hand boundary (higher amplitude and damping).

4.2 Nonlinear modal analysis

As established in [32], the amplitude-dependent modal properties can be extracted from the phase-resonant backbone curve, provided that strong modal interactions (e.g. due to closely-spaced or internally resonant natural frequen-

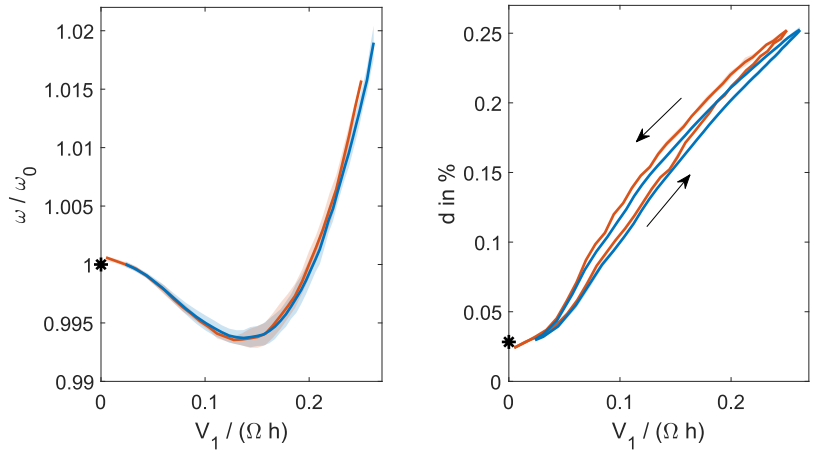

(a) (b)

Figure 13: (a) average nonlinear natural frequency and (b) nonlinear modal damping depending on the response level, identified with PLL testing (blue curve) and CBC (orange curve); compared to linear parameters identified during the linear modal analysis (∗)

cies) remain absent and damping is light. Here, the definition of a nonlinear mode in accordance with the extended periodic motion concept [57] is used. The modal frequency (or natural frequency) ω corresponds to the excitation frequency at phase resonance and is a direct output of the experiments. The nonlinear modal damping ratio δ is determined by following the idea that the power supplied by the excitation has to cancel the power dissipated by the system-inherent damping (see [32] for the details). Finally, the Fourier coefficients of the modal deflection shape are obtained by Fourier analysis. The fundamental harmonic component of this deflection shape is mass-normalized using the linear mass-normalized modal deflection shapes [32]. The average modal frequency and modal damping ratio are shown in Fig. 13a and Fig. 13b, respectively. As expected, the values of the parameters at low amplitude are consistent with the linear modal parameters.

Increasing damping ratio with amplitude is typical for micro-slip friction, which may also cause the increase in variability with amplitude shown in Fig. 12a. Although the damping has a standard deviation so small that it is barely visible in Fig. 13b, it exhibits an interesting hysteresis behavior. It is important to note that it is not a dynamical hysteresis, i.e. each point on the curve corresponds to a steady state periodic response identified during PLL testing or CBC. Rather, the behavior of the structure is different whether the amplitude is sequentially increased or decreased. We do not know the cause of this behavior, but a possi-

ble explanation could be linked to thermal effects analogous to the observations in [58].

4.3 FRC synthesis

FRCs can be synthesized from the nonlinear modal parameters presented in Section 4.2. It can be advantageous to do this as fewer periodic responses need to be measured compared to a direct FRC identification. Identifying FRCs both through synthesis and directly is done here as a cross-validation.

The synthesis relies on the single-nonlinear-mode theory: The frequency Ω of the FRC at a specific response amplitude is computed following [31]. The FRCs synthesized from the backbone curves are shown in Fig. 14. FRCs are synthesized from each backbone curve shown in Fig. 11a. They are parametrized by their phase lag such that there is a one-to-one correspondence between each point of the different curves: The successive FRCs are described by the functions $\omega_k(\phi_v)$ and $V_1(\phi_v)$ for the k^{th} curve. The standard deviation is computed for each phase lag value both in amplitude and frequency, and is shown as colored areas in Fig. 14.

The softening-hardening behavior is apparent in the FRCs. Under a forcing amplitude of 3 N, the FRCs are in the softening regime and are skewed toward lower frequencies. They include two saddle-node bifurcations. This indicates the existence of a branch of unstable orbits. Increasing the forcing amplitude above 3 N creates two more saddle-node bifurcations as the FRCs begin to be skewed towards higher frequencies. This hardening regime therefore includes two branches of unstable orbits, one due to softening and the other due to hardening. Recall that this leads to as much as four turning point bifurcations and and a stable high-level branch which can be unreachable by a conventional frequency response test (stepping or slowly sweeping the frequency and controlling only the excitation level).

4.4 FRC identification

FRCs are identified experimentally using PLL testing by following Algorithm 4. They are shown in blue in Fig. 15. The identification of FRCs is limited around the resonance peak. Further from resonance, a small phase lag variation implies a large frequency variation as illustrated in Fig. 1b. Consequently, even low phase lag uncertainty prevents the accurate identification of periodic responses. Additionally, periodic responses further from resonance have a low amplitude, leading to low signal-to-noise ratio in the measurement and high phase lag uncertainty, as explained in Section 3.3. Such a limitation is nuanced by the fact that interesting behavior is rarely expected far from resonance.

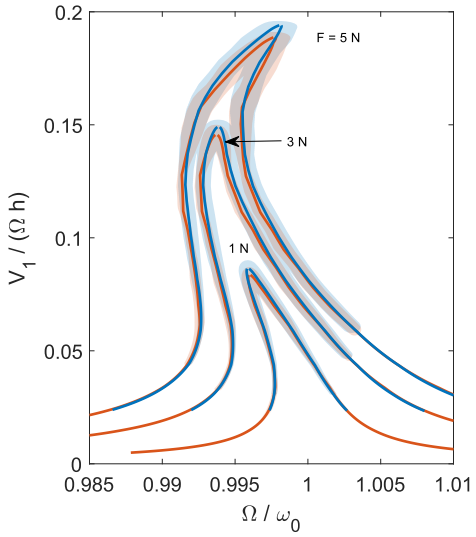

Figure 14: FRCs at varying excitation amplitudes synthesized from the average backbone curve identified with PLL testing (blue curve) and CBC (orange curve), and compared to the standard deviation from PLL testing (blue area) and CBC (orange area) data

The S-curves identified during CBC are shown in Fig. 16. Far away from resonance, the force level increases quickly, constituting a potential limitation of the method when applied to structures or equipment sensitive to high forcing. The phase lag along the S-curves is shown in Fig. 16b. The presence of two resonance points where $\phi_v = 0$ rad and the double-S shape of some S-curves results from the softening-hardening behavior of the system.

Processing S-curves into FRCs requires the approximation of the response surface from the measurement data. The experiments are not perfectly repeatable due to the inherent variability of the structure, it is therefore not appropriate to interpolate the S-curves into the response surface as was done in [24]. Rather, the response surface is approximated by a cubic spline surface with 10 equally spaced control points along the frequency dimension and 12 points along the response amplitude dimension. The location of the control points along the fundamental excitation force dimension is determined by minimizing the average distance between the surface and the data points. The data consists in the S-curves and the average backbone, useful to accurately capture the resonance region. The surface and data points are shown in Fig. 17.

The FRCs are finally extracted from the response surface as collections of periodic responses at constant excitation amplitudes. They are shown in orange in Fig. 15. To highlight the fact that the FRCs are not interpolations

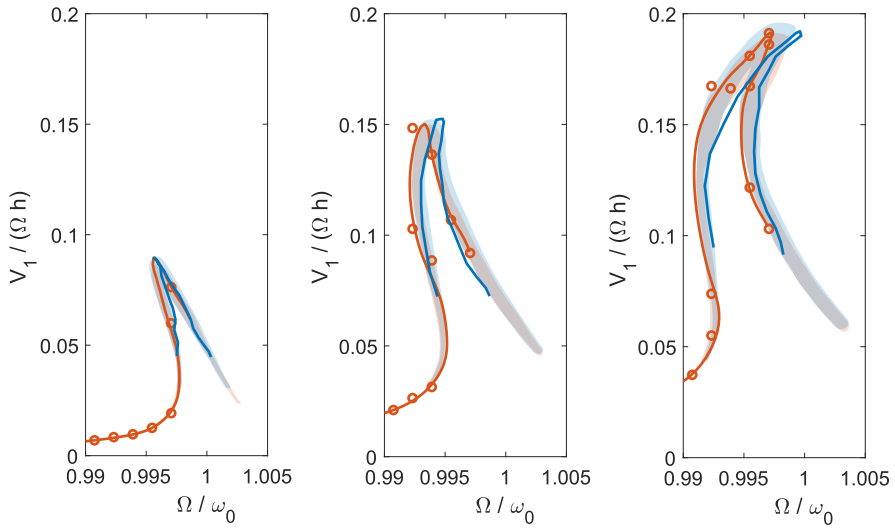

Figure 15: FRCs at excitation amplitudes (a) $F = 1$ N, (b) 3 N, and (c) 5 N identified experimentally with PLL testing (blue curve) and CBC (orange curve), compared to the S-curves identified with CBC (○) and to the standard deviation of the FRCs synthesized from backbone curves identified with PLL testing (blue area) and CBC (orange area)

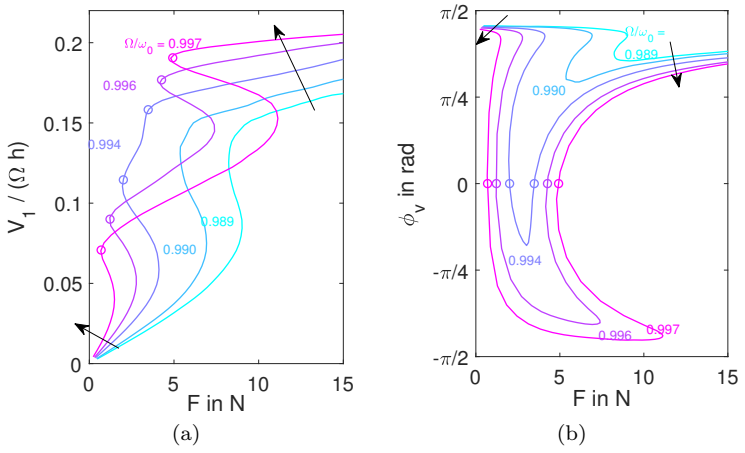

Figure 16: (a) Amplitude and (b) phase lag of S-curves identified experimentally during CBC for varying excitation frequencies; with highlighted resonance points at phase quadrature (○)

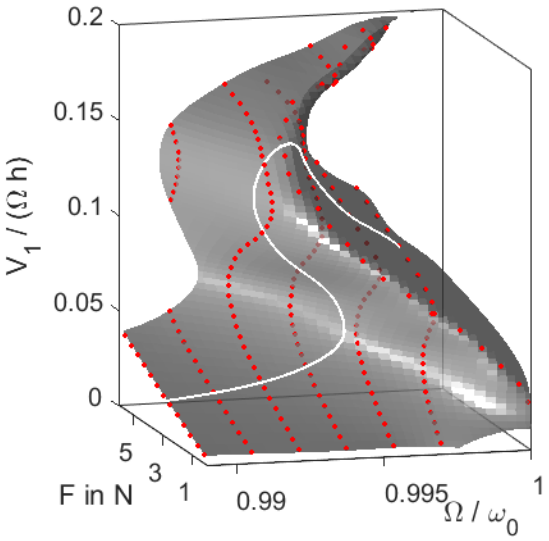

Figure 17: Response surface representing the response amplitudes of the system for varying excitation signals, approximated from the S-curves and the backbone identified experimentally with CBC (data points shown in orange and approximated FRC at $F = 3$ N in white)

but approximations, the intersection of the S-curves with the plane embedding the FRC are shown as orange circles. The resulting FRCs stay close to these intersections, showing an accurate approximation.

Although the identified FRCs—either directly using PLL testing or indirectly using CBC—show a slight difference in frequency, they lie within or very close to the standard deviation of FRCs synthesized from the backbones. In other words, such a difference in frequency is expected from the inherent variability of the system. This gives strong confidence in both the FRCs and the backbone curves identified using PLL testing and CBC. Finally, both methods successfully stabilize the unstable orbits in the FRCs.

5 Conclusion and future works

The aim of this article was to compare two recently developed methods capable of nonlinear modal characterization on the same structure. Both methods use feedback to control different experimental parameters. During phase-locked loop (PLL) testing, the phase lag between response and excitation signals is imposed by a controller. During control-based continuation (CBC), a controller

generates an excitation signal from the difference between a reference signal and the response of the structure.

Both PLL testing and CBC were shown capable of a successful characterization of the amplitude-dependent modal properties of the lowest-frequency bending mode of a thin beam possessing an intrinsic curvature when unstressed. The structure exhibits complex nonlinear hardening-softening dynamics and nonlinear micro-slip in the bolted joints, handled and identified successfully by both methods. The backbone identification—and subsequent nonlinear modal parameters and synthesized FRCs—and the FRC identification lead to consistent results obtained by PLL testing or CBC. The important difference between experimental data and model prediction shows the importance of control-based methods when predictive models are difficult to build.

It is difficult to compare quantitatively experimental duration using both methods. The tuning of the controllers plays a critical role in the dynamics of the system, e.g. the time needed to reach steady state. The parameters chosen in the continuation algorithms affect greatly the duration of experiments. An in-depth parameter study might be done to assess accurately performance of CBC and PLL testing but it is deemed outside the scope of this article. With these considerations, no significant difference in performance was observed in this study.

This article focused on bringing PLL testing and CBC together and presenting their different approaches in performing the same characterization. An equally relevant approach would set the methods apart by studying special cases where PLL testing or CBC might fail. Such cases are mentioned in this article and result from a difference in parametrization of the response surface exploited by both methods. On the one hand, modal interaction might render a parametrization by phase lag challenging [48] and a characterization by PLL testing incomplete. On the other hand, superharmonic resonance might prevent a parametrization by a single response harmonic [59] and a characterization by CBC might be incomplete. Further work looking into such particular systems will bring valuable elements to the discussion.

General methods are still lacking regarding the determination of control laws for control-based methods. Unless knowing in advance the nonlinearities of a system—i.e. building a model, defeating the purpose of the methods—controller gains are currently tuned heuristically. Further work looking into robust and general methods for building control laws is needed, possibly building upon the early work that has been done on the subject [51, 52].

Acknowledgements

G.A. is funded by the Fund for Research Training in Industry and Agriculture (FRIA) from the Fonds de la Recherche Scientifique (F.R.S - FNRS).

E.F. is funded by the AERMEC Laboratory at the Department of Aerospace and Mechanical Engineering, Politecnico di Torino. He gratefully acknowledges the support of AERMEC Laboratory and Prof. Stefano Zucca.

M.S. and M.K. acknowledge the funding by the Deutsche Forschungsgemeinschaft (DFG, German Research Foundation) [Project 402813361].

L.R. acknowledges the financial support of the Royal Academy of Engineering, Research Fellowship #RF1516/15/11.

References

[1] DJ Ewins. Modal testing: Theory and practice, 2nd eddition, 2000.

[2] Kenneth A Ramsey. Effective measurements for structural dynamics testing. *Sound and Vibration*, 9(11):24–34, 1975.

[3] Nuno Manuel Mendes Maia and Júlio Martins Montalvao e Silva. *Theoretical and experimental modal analysis*. Research Studies Press, 1997.

[4] Zhi-Fang Fu and Jimin He. *Modal analysis*. Elsevier, 2001.

[5] Rik Pintelon and Johan Schoukens. *System Identification: A Frequency Domain Approach*. John Wiley & Sons, 2010.

[6] Ondrej Rubes, Martin Brablc, and Zdenek Hadas. Nonlinear vibration energy harvester: Design and oscillating stability analyses. *Mechanical Systems and Signal Processing*, 125:170–184, 2019.

[7] Chiara Gastaldi, Johann Gross, Maren Scheel, Teresa M Berruti, and Malte Krack. Modeling complex contact conditions and their effect on blade dynamics. *Journal of Engineering for Gas Turbines and Power*, 143(1):011007, 2021.

[8] Gaëtan Kerschen, Keith Worden, Alexander F. Vakakis, and Jean Claude Golinval. Past, present and future of nonlinear system identification in structural dynamics. *Mechanical Systems and Signal Processing*, 20(3):505–592, 2006.

[9] Gaetan Kerschen, Young Sup Lee, Alexander F. Vakakis, D. Michael Mcfarland, and Lawrence A. Bergman. Irreversible passive energy transfer in coupled oscillators with essential nonlinearity. *SIAM Journal on Applied Mathematics*, 66(2):648–679, 2006.

[10] Jean Philippe Noël, L. Renson, C. Grappasonni, and G. Kerschen. Identification of nonlinear normal modes of engineering structures under broadband forcing. *Mechanical Systems and Signal Processing*, 74:95–110, 2016.

[11] Thibaut Detroux, Ludovic Renson, L. Masset, and Gaëtan Kerschen. The harmonic balance method for bifurcation analysis of nonlinear mechanical systems. *Conference Proceedings of the Society for Experimental Mechanics Series*, 1:65–82, 2016.

[12] Alexander F. Vakakis. *Normal Modes and Localization in Nonlinear Systems*. Springer Netherlands, 1 edition, 1996.

[13] Mehmet Kurt, Melih Eriten, D. Michael McFarland, Lawrence A. Bergman, and Alexander F. Vakakis. Methodology for model updating of mechanical components with local nonlinearities. *Journal of Sound and Vibration*, 357:331–348, 2015.

[14] K. Nandakumar and Anindya Chatterjee. Resonance, parameter estimation, and modal interactions in a strongly nonlinear benchtop oscillator. *Nonlinear Dynamics*, 40(2):149–167, 2005.

[15] Kestutis Pyragas. Continuous control of chaos by self-controlling feedback. *Physics letters A*, 170(6):421–428, 1992.

[16] Jan Sieber and Bernd Krauskopf. Control based bifurcation analysis for experiments. *Nonlinear Dynamics*, 51:356–377, 2008.

[17] Jan Sieber, Alicia Gonzalez-Buelga, Simon Neild, David Wagg, and Bernd Krauskopf. Experimental continuation of periodic orbits through a fold. *Physical Review Letters*, 100(24):244101, 2008.

[18] Ludovic Renson, A. D. Shaw, David A.W. Barton, and Simon Neild. Application of control-based continuation to a nonlinear structure with harmonically coupled modes. *Mechanical Systems and Signal Processing*, 120:449–464, 2019.

[19] V. Denis, M. Jossic, C. Giraud-Audine, B. Chomette, A. Renault, and O. Thomas. Identification of nonlinear modes using phase-locked-loop experimental continuation and normal form. *Mechanical Systems and Signal Processing*, 106:430–452, 2018.

[20] Ludovic Renson, Jan Sieber, David A.W. Barton, A. D. Shaw, and Simon Neild. Numerical continuation in nonlinear experiments using local Gaussian process regression. *Nonlinear Dynamics*, 98:2811–2826, 2019.

[21] Jan Sieber, Bernd Krauskopf, David Wagg, Simon Neild, and Alicia Gonzalez-Buelga. Control-based continuation of unstable periodic orbits. *Journal of Computational and Nonlinear Dynamics*, 6(1), 2011.

[22] David A.W. Barton and Stephen G. Burrow. Numerical continuation in a physical experiment: Investigation of a nonlinear energy harvester. *Journal of Computational and Nonlinear Dynamics*, 6(1):011010, 2011.

[23] Emil Bureau, Frank Schilder, Ilmar F Santos, Jon Juel Thomsen, and Jens Starke. Experimental bifurcation analysis for a driven nonlinear flexible pendulum using control-based continuation. In *7th European Nonlinear Dynamics Conference*, pages 24–29, July 2011.

[24] David A.W. Barton and Jan Sieber. Systematic experimental exploration of bifurcations with noninvasive control. *Physical Review E*, 87:052916, 2013.

[25] L. Renson, A. Gonzalez-Buelga, D. A.W. Barton, and S. A. Neild. Robust identification of backbone curves using control-based continuation. *Journal of Sound and Vibration*, 367:145–158, 2016.

[26] Gaëtan Abeloos, Ludovic Renson, Christophe Collette, and Gaëtan Kerschе. Stepped and Swept Control-Based Continuation using Adaptive Filtering. *Nonlinear Dynamics*, 2021.

[27] Ludovic Renson, David A.W. Barton, and Simon A. Neild. Experimental tracking of limit-point bifurcations and backbone curves using control-based continuation. *International Journal of Bifurcation and Chaos*, 27(1), 2017.

[28] Sebastian Mojrzisch, Jörg Wallaschek, and Jan Bremer. An experimental method for the phase controlled frequency response measurement of nonlinear vibration systems. *PAMM*, 12(1):253–254, 2012.

[29] Simon Peter and Remco I. Leine. Excitation power quantities in phase resonance testing of nonlinear systems with phase-locked-loop excitation. *Mechanical Systems and Signal Processing*, 96:139–158, 2017.

[30] Simon Peter, Maren Scheel, Malte Krack, and Remco I. Leine. Synthesis of nonlinear frequency responses with experimentally extracted nonlinear modes. *Mechanical Systems and Signal Processing*, 101:498–515, 2018.

[31] Stefan Schwarz, Lukas Kohlmann, Andreas Hartung, Johann Gross, Maren Scheel, and Malte Krack. Validation of a Turbine Blade Component Test With Frictional Contacts by Phase-Locked-Loop and Force-Controlled Measurements. *Journal of Engineering for Gas Turbines and Power*, 142(5):051006, 2020.

[32] Maren Scheel, Simon Peter, Remco I. Leine, and Malte Krack. A phase resonance approach for modal testing of structures with nonlinear dissipation. *Journal of Sound and Vibration*, 435:56–73, 2018.

[33] Maren Scheel, Tobias Weigele, and Malte Krack. Challenging an experimental nonlinear modal analysis method with a new strongly friction-damped structure. *Journal of Sound and Vibration*, 485:115580, 2020.

[34] M. Link, M. Böswald, S. Laborde, M. Weiland, and A. Calvi. Non-linear experimental modal analysis and application to satellite test data. In *Proceedings of COMPDYN 2011 - 3rd International Conference on Computational Methods in Structural Dynamics & Earthquake Engineering*, pages 26–28, 2011.

[35] Taylan Karaağaçlı and H. Nevzat Özgüven. Experimental modal analysis of nonlinear systems by using response-controlled stepped-sine testing. *Mechanical Systems and Signal Processing*, 146, 2021.

[36] Taylan Karaağaçlı and H. Nevzat Özgüven. A frequency domain nonparametric identification method for nonlinear structures: Describing surface method. *Mechanical Systems and Signal Processing*, 144:106872, 2020.

[37] Young S. Lee, Alexander F. Vakakis, Lawrence A. Bergman, D. Michael McFarland, and Gaëtan Kerschen. Suppressing aeroelastic instability using broadband passive targeted energy transfers, part 1: Theory. *AIAA Journal*, 45(3):693–711, 2007.

[38] G. Zhao, A. Paknejad, G. Raze, A. Deraemaeker, G. Kerschen, and C. Collette. Nonlinear positive position feedback control for mitigation of nonlinear vibrations. *Mechanical Systems and Signal Processing*, 132:457–470, 2019.

[39] M. R.W. Brake, C. W. Schwingshackl, and P. Reuß. Observations of variability and repeatability in jointed structures. *Mechanical Systems and Signal Processing*, 129:282–307, 2019.

[40] Lawrence N. Virgin. *Introduction to Experimental Nonlinear Dynamics*. Cambridge University Press, 2000.

[41] David A. Ehrhardt, Robert J. Kuether, and Matthew S. Allen. Nonlinear normal modes in finite element model validation of geometrically nonlinear flat and curved beams. *56th AIAA/ASCE/AHS/ASC Structures, Structural Dynamics, and Materials Conference*, 2015.

[42] Yenny Chandra, Richard Wiebe, Ilinca Stanciulescu, Lawrence N. Virgin, Stephen M. Spottswood, and Thomas G. Eason. Characterizing dynamic transitions associated with snap-through of clamped shallow arches. *Journal of Sound and Vibration*, 332(22):5837–5855, 2013.

[43] Yenny Chandra, Ilinca Stanciulescu, Lawrence N. Virgin, Thomas G. Eason, and Stephen M. Spottswood. A numerical investigation of snap-through in a shallow arch-like model. *Journal of Sound and Vibration*, 332(10):2532–2548, 2013.

[44] M.I. McEwan, J.R. Wright, J.E. Cooper, and A.Y.T. Leung. A Combined Modal/Finite Element Analysis Technique for The Dynamic Response of a Non-linear Beam to Harmonic Excitation. *Journal of Sound and Vibration*, 243(4):601–624, jun 2001.

[45] Malte Krack and Johann Gross. *Harmonic Balance for Nonlinear Vibration Problems*. Mathematical Engineering. Springer International Publishing, Cham, 2019.

[46] C.S. Koukourlis, V.K. Trigonidis, and John N. Sahalos. Differential synchronous demodulation for small signal amplitude estimation. *IEEE Transactions on Instrumentation and Measurement*, 1993.

[47] Emil Bureau, Frank Schilder, Ilmar Ferreira Santos, Jon Juel Thomsen, and Jens Starke. Experimental bifurcation analysis of an impact oscillator - Tuning a non-invasive control scheme. *Journal of Sound and Vibration*, 332(22):5883–5897, 2013.

[48] R. J. Kuether, L. Renson, T. Detroux, C. Grappasonni, G. Kerschen, and M. S. Allen. Nonlinear normal modes, modal interactions and isolated resonance curves. *Journal of Sound and Vibration*, 351:299–310, 2015.

[49] Ludovic Renson. Identification of backbone curves and nonlinear frequency responses using control-based continuation and local gaussian process regression. In Gaetan Kerschen, Matthew R.W. Brake, and Ludovic Renson, editors, *Nonlinear Structures & Systems, Volume 1*, pages 83–85, Cham, 2021. Springer International Publishing.

[50] S. Peter, F. Schreyer, P. Reuss, and L. Gaul. Consideration of local stiffening and clearance nonlinearities in coupled systems using a generalized Harmonic Balance Method. *Proceedings of ISMA 2014 - International Conference on Noise and Vibration Engineering and USD 2014 - International Conference on Uncertainty in Structural Dynamics*, pages 3097–3110, 2014.

[51] Mrdjan Jankovic. Control lyapunov-razumikhin functions and robust stabilization of time delay systems. *IEEE Transactions on Automatic Control*, 46(7):1048–1060, 2001.

[52] Yang Li and Harry Dankowicz. Adaptive control designs for control-based continuation of periodic orbits in a class of uncertain linear systems. *Nonlinear Dynamics*, 103(3):2563–2579, 2021.

[53] Kiam Heong Ang, Gregory Chong, and Yun Li. PID control system analysis, design, and technology. *IEEE Transactions on Control Systems Technology*, 13(4):559–576, 2005.

[54] Maryam Ghandchi-Tehrani, Lawrence I. Wilmshurst, and Stephen J. Elliott. Bifurcation control of a Duffing oscillator using pole placement. *JVC/Journal of Vibration and Control*, 21(14):2838–2851, 2015.

[55] Jacopo Marconi, Paolo Tiso, Davide E. Quadrelli, and Francesco Braghin. A higher-order parametric nonlinear reduced-order model for imperfect structures using Neumann expansion. *Nonlinear Dynamics*, 2021.

[56] Erhan Ferhatoglu and Stefano Zucca. On the non-uniqueness of friction forces and the systematic computation of dynamic response boundaries for turbine bladed disks with contacts. *Mechanical Systems and Signal Processing*, 160:107917, 2021.

[57] Malte Krack. Nonlinear modal analysis of nonconservative systems: Extension of the periodic motion concept. *Computers and Structures*, 154:59–71, 2015.

[58] Sebastian Mojrzisch and Jens Twiefel. Phase-controlled frequency response measurement of a piezoelectric ring at high vibration amplitude. *Archive of Applied Mechanics*, pages 1–7, 2015.

[59] Martin Volvert and Gaetan Kerschen. Phase resonance nonlinear modes of mechanical systems. *Journal of Sound and Vibration*, 511, 2021.